

Simulating wind-affected snow accumulations at catchment to basin scales



Adam Winstral ^{a,*}, Danny Marks ^a, Robert Gurney ^b

^a USDA-ARS Northwest Watershed Research Center, 800 Park Blvd., Suite 105, Boise, ID 83712, USA

^b University of Reading, ESSC, 3 Earley Gate, Reading, Berks RG6 6AL, UK

ARTICLE INFO

Article history:

Available online 12 September 2012

Keywords:

Snow
Wind
Drift
Distributed
Model
Precipitation

ABSTRACT

In non-forested mountain regions, wind plays a dominant role in determining snow accumulation and melt patterns. A new, computationally efficient algorithm for distributing the complex and heterogeneous effects of wind on snow distributions was developed. The distribution algorithm uses terrain structure, vegetation, and wind data to adjust commonly available precipitation data to simulate wind-affected accumulations. This research describes model development and application in three research catchments in the Reynolds Creek Experimental Watershed in southwest Idaho, USA. All three catchments feature highly variable snow distributions driven by wind. The algorithm was used to derive model forcings for *Isnobal*, a mass and energy balance distributed snow model. Development and initial testing took place in the Reynolds Mountain East catchment (0.36 km^2) where R^2 values for the wind-affected snow distributions ranged from 0.50 to 0.67 for four observation periods spanning two years. At the Upper Sheep Creek catchment (0.26 km^2) R^2 values for the wind-affected model were 0.66 and 0.70. These R^2 values matched or exceeded previously published cross-validation results from regression-based statistical analyses of snow distributions in similar environments. In both catchments the wind-affected model accurately located large drift zones, snow-scoured slopes, and produced melt patterns consistent with observed streamflow. Models that did not account for wind effects produced relatively homogenous SWE distributions, R^2 values approaching 0.0, and melt patterns inconsistent with observed streamflow. The Dobson Creek (14.0 km^2) application incorporated elevation effects into the distribution routine and was conducted over a two-dimensional grid of 6.67×10^5 pixels. Comparisons with satellite-derived snow-covered-area again demonstrated that the model did an excellent job locating regions with wind-affected snow accumulations. This final application demonstrated that the computational efficiency and modest data requirements of this approach are ideally suited for large-scale operational applications.

Published by Elsevier Ltd.

1. Introduction

Alpine snow distributions typically exhibit high spatial variability with consequent strong impacts on ecohydrologic processes [1–8]. The heterogeneity of snow distributions is a product of the differential mass and energy fluxes created when atmospheric processes interact with the complex topography and diverse vegetation patterns often present in these regions. While the spatially varying energy fluxes produce differential melt, sublimation, and condensation, these effects are generally secondary compared to elevation- and wind-affected mass fluxes (see [9–11] and others). Elevation-induced orographic effects produce higher precipitation rates at higher elevations. Winds further affect snow distribution patterns moving snow from wind exposed to

wind-sheltered areas via the processes of preferential deposition [12], saltation, and suspension [13,14]. In alpine basins, it is not uncommon to find windswept, snow-free ridgelines less than 100 meters away from snowdrifts containing meters of snow [3,5,15,16].

Orographic effects on precipitation modify both snow and rain distributions. Elevation-based trends have been the subject of much research and several methods of accounting for these effects in hydrologic models have been proposed (e.g. [17–19]). The wind-influenced processes affecting snow distributions however, are complex, less well understood, and challenge physically explicit solutions. Preferential deposition or inhomogeneous precipitation [12] is a recently introduced concept whereby turbulence in the lower atmosphere affects snowfall. Strong winds and updrafts over wind-exposed slopes reduce particle deposition velocities. Deposition rates decrease and a concentration of air-borne snow particles is produced. When the snow-concentrated air parcel moves over a

* Corresponding author. Tel.: +1 208 422 0739; fax: +1 208 334 1502.

E-mail address: adam.winstral@ars.usda.gov (A. Winstral).

leeward slope, wind speeds and updrafts decrease and snow is preferentially deposited. Erosion and redistribution of already deposited snow has been referred to as snow redistribution [13,14] or snow-drifting [15]. Erosion occurs when the applied wind shear stress exceeds the surface shear strength of exposed snow grains mobilizing the grains into creep, saltation, and suspension modes. Entrained particles are redeposited in areas with reduced winds or sublimate.

Modeling solutions have contributed much to the understanding of the physical processes that control wind-induced snow patterns. Lehning et al. [12] introduced the concept of inhomogeneous precipitation based on model solutions and observations of snow distribution over an isolated ridge with steep slopes. Physically-based snow redistribution models such as PBSM [13] and SnowTran3D [14] explicitly transport snow from exposed to sheltered areas. PBSM and SnowTran3D have led to important insights on threshold shear stresses, transport and sublimation rates, and the determination of scour and deposition zones. Due to the computational challenges of explicitly modeling these complex processes applications of the aforementioned models have been largely limited to small research areas with applications over larger areas requiring substantial simplifications (e.g. [20–22]).

Researchers have proposed and tested simpler methods for characterizing the effects of wind on snow distributions to broaden the reach of potential applications. Most of these efforts have focused on establishing relationships between terrain structure and wind effects. Blöschl et al. [23], Cline [24], Lapen and Martz [25], Purves et al. [26], Hartman et al. [27], and Winstral et al. [28] all successfully applied terrain parameters as proxies for wind-affected snow distributions. In one way or another, these studies sought to correlate the spatial patterns generated by the terrain parameterizations with observed snow patterns. Winstral and Marks [5] took these advances a step further applying terrain parameterizations along with vegetation data and intra-storm meteorology to distribute explicit snow forcings to a distributed snow model. The derived snow distributions were computationally efficient and greatly improved model simulations of snow distribution and melt.

Winstral and Marks [5] based their work on two terrain parameters, one a measure of upwind slopes (S_x) and the other a measure of upwind breaks in slope (S_b). As a predictor of snow distributions in non-forested alpine regions, S_x performed better than parameters based on curvature, fetch, and average upwind slopes [29]. The strong relationship between S_x and wind-affected snow distributions has been demonstrated in several studies [7,28–31]. Site-to-site differences in S_x were also significant predictors of between-site wind speed differences [32]. Winstral and Marks [5] used S_x to linearly interpolate wind-sheltered and wind-exposed snow observations to other locations while S_b determined enhanced accumulation areas (i.e. drifts). Drift accumulations varied as a function of intra-storm totals at sheltered and exposed sites. The authors showed that these parameters were effective at predicting a very heterogeneous snow distribution, yet as presented these methods required data from proximal sheltered and exposed locations – data rarely available outside of research watersheds.

This research aims to expand upon the techniques of Winstral and Marks [5] to develop tools that improve and expand snow modeling capabilities while capturing the hydrologically relevant aspects of snow distribution heterogeneity using commonly available data. Snow accumulations at sheltered sites are not affected by wind and is equivalent to precipitation – a commonly measured variable that can also be estimated from numerical weather models (e.g. U.K. Met Office's convective-scale NWP) or radar observations. Data on snow accumulation at exposed sites however, are rarely available. In lieu of exposed site data, which were

used as interpolative end-members in Winstral and Marks [5], we hypothesize that wind speeds, terrain, and vegetation can be used to scale “sheltered” snow accumulations to accumulations at wind-affected sites. Wind speed has a direct correlation to wind shear stress, the forcing behind wind-induced redistribution of snow. Modeled wind speeds have been used to parameterize the seasonal effects of preferential deposition as well [15]. Upwind terrain affects not only the horizontal component of winds [32], but also the vertical component – a key contributing factor to preferential deposition.

This research assessed the relationships of snow accumulation rates to wind speeds, terrain structure, and vegetation at Reynolds Mountain East (0.36 km^2), an intensively monitored research watershed. Observations extended across a broad range of exposures and snow accumulations. Wind speeds and snow depth were continuously monitored at three weather stations and snow-water-equivalent (SWE) was manually surveyed across the entire catchment twice a year. These relationships were used as the basis for a computationally efficient means of distributing wind-affected snow accumulations to force *Isnobal* [33], a mass- and energy-balance snow model. *Isnobal*-modeled SWE distributions with and without wind-affected snow accumulations were then compared to observed distributions at Reynolds Mountain East. Melt simulations were compared to streamflow as well. The model was further tested at two other RCEW watersheds. Wind strongly affects the distribution of snow and ultimately streamflow in these catchments as well. At the Upper Sheep Creek catchment (0.27 km^2) simulations were likewise compared to basin-wide measured SWE distributions to directly assess how the modeling techniques calibrated at Reynolds Mountain East performed in an independent application. Simulations at the larger Dobson Creek catchment (14.0 km^2) demonstrated how elevation gradients could be incorporated into the modeling procedure. In each simulation *Isnobal* was forced with precipitation data solely from wind-sheltered stations with similar site characteristics to those of most mountain observatories.

2. Field sites and data

2.1. Reynolds Mountain East

Reynolds Mountain East is where relationships between snow accumulation rates, wind speeds, terrain, and vegetation were investigated. Reynolds Mountain East is a unique headwater catchment located within the Reynolds Creek Experimental Watershed in southwestern Idaho, USA (Fig. 1). Elevation ranges from 2027 to 2137 masl and the average slope is 8.2° . Vegetation consists of aspen, fir, willow, and a mix of sagebrushes ranging in height from cm's to 2 m. Mean annual precipitation is 1020 mm with approximately 75% occurring as snow [34]. Prevailing winds are typically out of the southwest with wintertime mean resultant wind directions generally between 225° and 230° .

Though covering an area of only 0.36 km^2 , varied terrain and vegetation combine to produce strongly heterogeneous snow distributions. Meters of snow can be present in drifts whereas nearby wind-exposed locations rarely reach depths exceeding 10 cm. The varied snow distribution has a strong effect on streamflow [5], vegetation, soil moisture, and recharge [6]. Reynolds Mountain East has been instrumented with a unique suite of sensors designed to capture the strong meteorological gradients that generate the varied snow distribution in this catchment. Three fully-instrumented meteorological stations measuring air temperature, relative humidity, wind speed and direction, solar radiation, and precipitation were used in this study. The grove site (GR, $\bar{u} = 2.0 \text{ ms}^{-1}$) is located in a wind-sheltered, forest opening characteristic of most mountain weather stations (Note: \bar{u} is mean wind

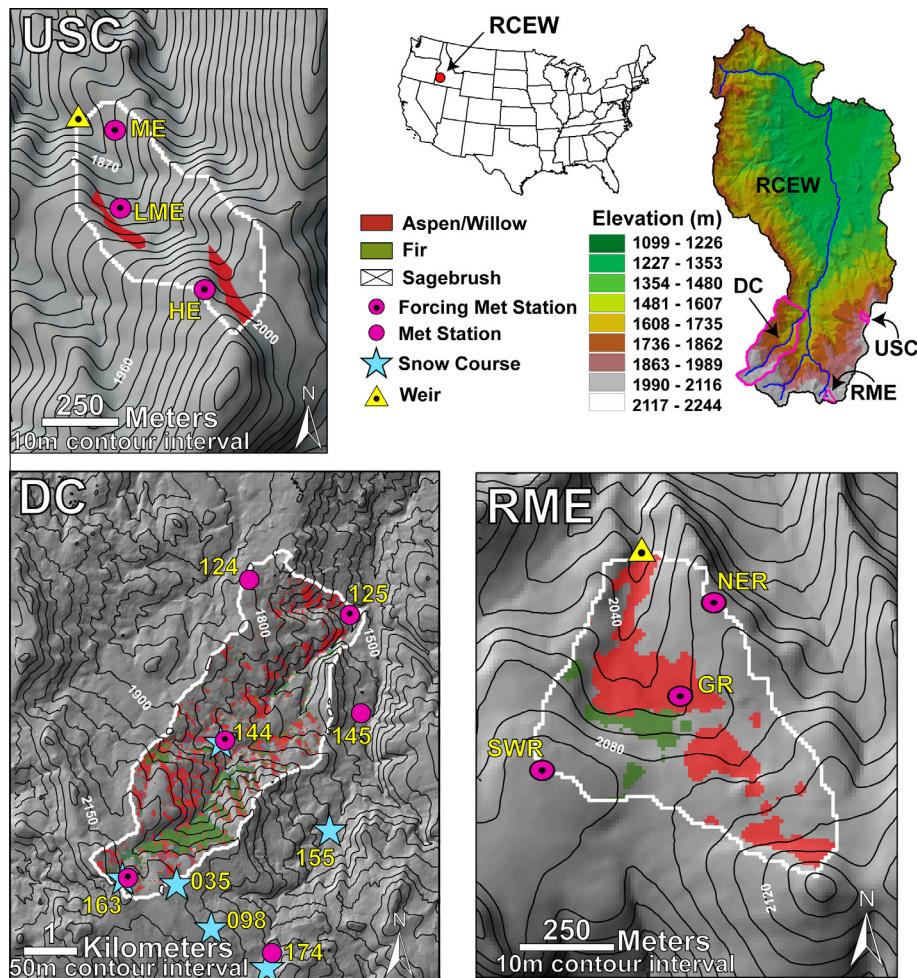


Fig. 1. The sites of the three model applications: Reynolds Mountain East (RME), Upper Sheep Creek (USC), and Dobson Creek (DC). The non-forcing stations and snow courses in DC were used for model validation.

speed during the study period.). In the spatial modeling the only precipitation data used to drive the model came from site GR. The two other sites are on open ridges with varying exposures: the southwest (SWR, $\bar{u} = 4.7 \text{ ms}^{-1}$) and northeast (NER, $\bar{u} = 6.2 \text{ ms}^{-1}$) ridge sites. The SWR site is surrounded by sparse

sagebrush 50–100 cm in height. The NER site is surrounded by bare rock. Both ridge sites accumulate less snow than the GR site with accumulations rarely exceeding 10 cm at the NER site (Fig. 2). Precipitation, wind, and snow depth data from these sites were used to assess snow accumulation differences.

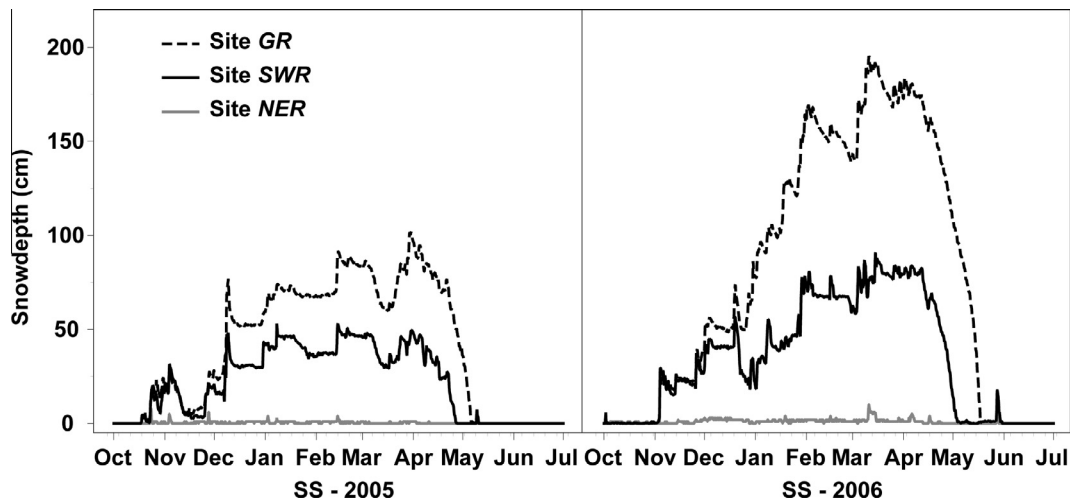


Fig. 2. The very different snow accumulation regimes at the three meteorological stations in Reynolds Mountain East. Accumulation at the SWR site mirrors that of the sheltered GR site early in the season when shrubs remain exposed reducing surface winds.

Manual snow surveys captured the full heterogeneity of snow distribution in Reynolds Mountain East and were the only data available from accumulation-enhanced or drift areas. Surveys were conducted twice a year – mid-winter and early spring. The catchment's size and absence of avalanche danger allowed for full catchment coverage. A 30 m grid-based sampling design was employed. Two depth samples were taken in each 30 m cell – one at the center and one offset from the center by 10 m in a randomly selected cardinal direction. A total of 840 depth measurements were made in each survey. Snow density measurements were taken with a Federal Mt. Rose core sampler with spring balance in order to convert the depth measurements to snow-water-equivalent (SWE). While density measurements are much more time consuming than depth measurements, the coefficient of variation for snow density is far less than that of snow depth and the density distribution can be accurately described with fewer samples [35]. Based on prior survey data it is been found that any density trend in this catchment will be related to snow depth. In order to evaluate density-to-depth trends, approximately 30 density samples were collected in each survey using a depth-stratified random sampling scheme. A density-to-depth linear regression with potential steps for low accumulation areas with a predominance of new snow and another for maximal densities in the deep drifts was evaluated for each survey period. If the relationship through the mid-range of depths was statistically significant ($p < 0.05$), said relationship along with the potential low- and high-end steps was used to distribute densities and register a snow-water-equivalent value to each depth measure. Otherwise, the mean of all density samples was applied. The snow survey data were used to calibrate the snow accumulation algorithm and evaluate *Isnobal* simulations.

A 10 m grid cell digital elevation model (DEM) served as the basis for terrain analysis and modeling. The 10 m DEM was aggregated from a 1 m grid cell LiDAR (light detection and ranging) derived DEM. The aggregation compensated for ground-determination problems in areas with low-lying vegetation and the 10 m grid-scale coincides with prior scale-based terrain analyses used to simulate wind fields (see [32]). Data from two snow seasons, 2004–2005 (SS-2005) and 2005–2006 (SS-2006), were evaluated. Precipitation was below average in SS-2005 (78%) and above average in SS-2006 (133%).

2.2. Upper Sheep Creek

The Upper Sheep Creek catchment (Fig. 1) – featuring nearly identical instrumentation, data availability, and size as Reynolds Mountain East – offered a directly comparable and quantifiable test of model transferability. Upper Sheep Creek has a long history of hydrological research related to soil moisture, water balance, and snow accumulation and melt [3,36–39]. The catchment has an area of 0.26 km² and an elevation range of 1837–2023 masl. Prevailing winds are typically out of the west-southwest producing large drifts on northeast-facing slopes. Just prior to the study year a prescribed burn eliminated all of the existing mixed sagebrush communities that had been present in 90% of the watershed. The remaining 10% of the basin consisted of aspens, which were burned but remained standing through the test period.

Differences in snow accumulation in Upper Sheep Creek are extreme – water availability is concentrated in lee slope drifts with very little snow accumulating on wind-exposed slopes. Flerchinger and Cooley [36] in a 10-year water balance study of Upper Sheep Creek stated, “it is imperative to account for the variability in precipitation and snow redistribution in addressing the hydrologic processes occurring in the watershed.” Luce et al. [3] took a streamflow focus and found that accounting for the spatially variable snow distribution in Upper Sheep Creek was required to properly match simulated meltwater inputs to streamflow.

Similar to Reynolds Mountain East, data from three fully instrumented meteorological stations with varied exposures and snow accumulations were available. The stations ranged in wind exposure from low-to-moderate (*LME*, $\bar{u} = 3.3 \text{ ms}^{-1}$) and moderate (*ME*, $\bar{u} = 4.7 \text{ ms}^{-1}$) through high (*HE*, $\bar{u} = 8.0 \text{ ms}^{-1}$). Precipitation values were distributed based solely on undercatch-corrected hourly precipitation [40] at the *LME* site. Validation data consisted of distributed SWE data from manual field surveys conducted in a similar fashion to the Reynolds Mountain East surveys. Due to the importance of the drifts to the hydrology of Upper Sheep Creek, additional “offset” depth samples were collected at each drift sampling site.

The aim of the Upper Sheep Creek application was to test the transferability of the snow accumulation model. *Isnobal* simulations, forced with both the distributed snow accumulation algorithm developed at Reynolds Mountain East and spatially constant snow accumulation forcings, were compared to the SWE distributions observed in the manual surveys. Upper Sheep Creek and Reynolds Mountain East have similarly designed observation networks ensuring that the forcing and validation data were of similar scope and quality – truly testing transferability. In the subsequent application over the larger Dobson Creek catchment the range and spatial resolution of observations for forcing and validating *Isnobal* were far more limited.

Modeling took place over the course of the 2008 snow season (SS-2008). Precipitation during SS-2008 was just below normal at 90% of the 40-year mean. Similar to the Reynolds Mountain East modeling, a 10 m grid-scale DEM aggregated from a 1 m LiDAR-derived product was the basis for modeling at a one-hour timestep.

2.3. Dobson Creek

The Dobson Creek catchment has an elevation range of 1474 to 2244 masl and covers an area of 14.0 km². The applications at Reynolds Mountain East and Upper Sheep Creek were conducted over small areas with limited elevation differences in order to focus on the effects of terrain and vegetation on snow accumulation. Along with strong terrain and vegetation influences on snow accumulation, elevation also plays a critical role on precipitation patterns in Dobson Creek. Precipitation amounts, as well as phases vary widely between the low and high elevations [41]. Additionally, whereas Reynolds Mountain East and Upper Sheep Creek had wind data from sites with widely varying exposures to bolster the accuracy of the simulated wind fields, all of the available forcing data for Dobson Creek came from wind-sheltered locations. Forcing the model with data solely from wind-sheltered locations along with the incorporation of elevation effects into the modeling procedures develops a foundation for operationally-realistic applications.

Vegetation in Dobson Creek is a mix of fir, aspen, mixed sagebrush, and scattered juniper (Fig. 1). Fir trees predominate on north-facing slopes in the middle to high elevations. Aspen groves are found in wetter areas of the catchment particularly those associated with high snow accumulations and sagebrushes are concentrated in drier, low accumulation areas. Prevailing winds out of the west-southwest produce large snowdrifts on east and northeast facing slopes at the upper elevations.

Data from three meteorological stations (Fig. 1) with similar instrumentation to the stations in Reynolds Mountain East and Upper Sheep Creek were used to derive the *Isnobal* forcings. Though these three sites did not capture wind-exposure gradients, they did adequately capture elevation gradients – only 4% of the catchment occupied elevations outside those bounded by the sites. Modeling took place during SS-2006, which was wetter than average and featured a large rain-on-snow event in late December [41]. The wind-corrected precipitation totals at the three sites during

SS-2006 were 698 mm (1506 masl), 988 mm (1815 masl), and 1261 mm (2169 masl). Model scale was once again 10 m; however this DEM was derived from standard US Geologic Survey contours by a commercial company (Peerless Management Systems, Springfield, OR, USA).

Validation of spatial models at scales such as these presents considerable challenges [42]. Validation data at Dobson Creek were a combination of point and remotely sensed data. Point data consisted of bi-monthly sampled SWE at six snow courses and continuously monitored snow depth at six weather stations in and around the catchment (Fig. 1). A processed Landsat TM image depicting snow-covered-area in late spring was used to validate the simulated pattern of snow-enhanced and snow-inhibited regions in the upper catchment. The digital number (DN) values in the 30 m resolution Landsat TM image were converted to reflectances using guidelines set forth in NASA's *Landsat 7 Science Data Users Handbook* [43]. Snow-covered and snow-free areas were classified using a Normalized Differential Snow Index (NDSI) following the procedures of Hall et al. [44] and Dozier [45]. The combination of volumetric ground-based point measurements and spatial snow-cover patterns is widely considered sufficient for validating spatial models at this scale (e.g. [5,23,46]).

The simulations of differential snow accumulation and melt in Dobson Creek represent a considerable snow modeling achievement. These simulations were the first to simulate drift, scour, preferential deposition, and snowmelt over this large an area at such fine temporal (hourly) and spatial (10 m) resolutions. In this application, all of the forcings including the all-important snow accumulation gradients were modeled over a 67 km² rectangular grid of 893 × 747 pixels that included a substantial buffer around the catchment (the entire rectangular domain in Fig. 1). While more complex three-dimensional solutions of wind-affected snow accumulations including energetics have been achieved at similar spatio-temporal resolutions, their two-dimensional extent is often compromised as a result (e.g. [8,20,47–49]).

3. Methods

The terrain parameters, S_x and S_b , are respectively measures of maximum upwind slopes and upwind breaks in slope. Differences in S_x have been shown to be an excellent predictor of wind-affected snow distributions [5,28–31] and were significantly related to observed wind speed differences [32]. In this research numerical relationships between these terrain parameters and wind-affected snow accumulations are further examined. The derivations of S_x and S_b are briefly summarized here. Greater details can be found in Winstral et al. [28].

The S_x algorithm examines all cells along a fixed search line emanating from the cell of interest to determine which cell has the greatest upward slope relative to the cell of interest. Negative S_x values indicate that the cell of interest is the highest cell along the search line making it topographically exposed relative to the search direction. Positive S_x values indicate the presence of sheltering terrain. The d_{max} variable controls the extent of the search line and can have a substantial effect on S_x (see [32], also demonstrated in Section 4.1.1). Winstral et al. [28] added a *height* variable to S_x derivations whereby an offset elevation was added to cells of interest. The increased cell heights allow the terrain parameter to "see" more prominent terrain further along the search line as the effects of small, proximal terrain perturbations are reduced (Fig. 3).

The S_b parameter measures slope differences between local and outlying topography to gauge upwind breaks in slope capable of producing flow separation zones [5]. S_b is determined using two applications of the S_x algorithm to determine local and outlying

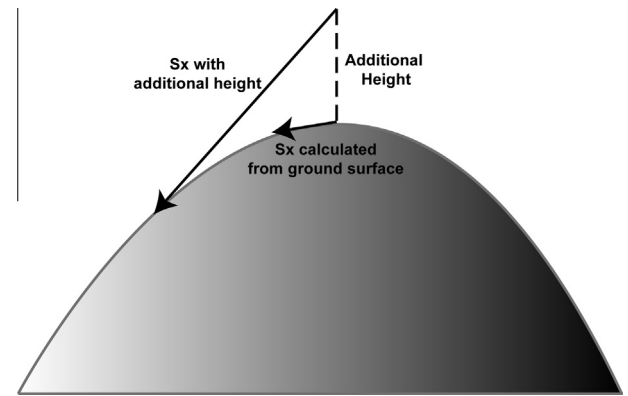


Fig. 3. The effect of additional "above-ground-heights" on S_x calculations for a convex ridge. S_x calculated from the ground elevation indicates a slightly exposed site. The additional height produces an S_x value characteristic of a very exposed site.

values of S_x . Basically, the calculation of the outlying S_x begins where the local determination ends. The difference between these two measures provides a measure of slope changes.

S_x and S_b were determined in five degree increments from 0° to 355°. At each 5° incremented direction, S_x and S_b averages were obtained across a 30° upwind window to assess a wider range of topographic features. This process established a library of \bar{S}_x and \bar{S}_b images in 5° increments that were retrieved based on observed wind directions.

The automated measurements from the three meteorological stations at Reynolds Mountain East aptly captured storm event dynamics. These sites cover a range in accumulations from extremely exposed (NER) to moderately exposed (SWR) to sheltered with no wind effects (GR). This range will be referred to as accumulation-inhibited – snow accumulations up to but not exceeding what would typically be found at that elevation in the absence of wind effects. Accumulation-enhanced sites on the other hand, are areas where wind has acted to increase accumulation. The only available data from accumulation-enhanced sites consisted of the snow survey data. The survey data however, represent the cumulative effects of all prior storms and weather events. Hence, a two-step procedure was used in model development. In the first step, storm data from the three meteorological stations along with the survey data were evaluated to develop a method for distributing measured precipitation from prototypical sites such as GR to accumulation-inhibited sites. In the second step, *Isnobal* [33], a proven mass and energy balance snow model (see [5,50,51]) and others), was initiated at start of the snow season to account for the cumulative weather effects contained in the survey data. A drift accumulation ratio (DAR) leveraged from GR site precipitation was then calibrated that best matched *Isnobal*-modeled SWE to surveyed SWE at the accumulation-enhanced sites.

Groundwork for the first step was to best match \bar{S}_x , in terms of d_{max} and *height*, to the observed snow accumulation patterns at accumulation-inhibited sites. The accumulation-optimized \bar{S}_x parameter was then included with the meteorological station data to establish numerical relationships for the snow-restricted portion of the snow accumulation distribution algorithm. Proceeding in this fashion ensured that spatial considerations were accounted for in a numerical model produced from the station data. Conversely, optimizing \bar{S}_x to the meteorological station data may have compromised the spatial simulations, which were the primary concern of this research.

The d_{max} and *height* variables within S_x were varied to best match spatial patterns of \bar{S}_x to observed SWE distributions. \bar{S}_x der-

iations for the calibration were focused on the prevailing storm wind direction of 225° with a 30° averaging window. The d_{max} variable was varied from 100 to 400 m in 50 m increments and the height variable from 0 to 4 m in one meter increments. \bar{S}_x distributions were compared to the February survey data as the mid-winter snow distributions have a stronger snow distribution signal and reduced melt influences compared to the spring distributions. All measured SWE values equal to or less than observed SWE at the GR site were normalized by GR site SWE and correlated to the various \bar{S}_x derivations. Only sites without strong vegetation influences (i.e. sagebrush and non-vegetated sites) were included in the analysis to best isolate terrain effects on accumulation. Vegetation effects on accumulation are accounted for in a subsequent model step (Section 4).

Snow accumulations and meteorological data at the GR, SWR, and NER sites were then summarized for storm periods during SS-2005 and SS-2006 to assess accumulation dependencies on wind speed and the accumulation-optimized \bar{S}_x . The sagebrush and shrubs at site SWR limit wind effects on snow accumulations until buried by snow (Fig. 2). Hence, only storm events occurring between 01-Dec and 30-April were considered in the analysis. For each storm event, total snow accumulation, mean dew point temperature, mean wind speed, and resultant mean wind direction were calculated at each site. Based on extensive snow modeling conducted at the GR and SWR sites (e.g. [5,52,53]) it's been shown that undercatch-corrected precipitation (see [54,40]) accurately portrays snow accumulation at the GR site while by sheer serendipity, uncorrected alter-shielded precipitation provides an excellent estimate at the windier SWR site. At the very exposed NER site, even the unshielded gauge overestimated snow accumulation. The best estimate of snow accumulation at the NER site consisted of the observed change in depth converted to SWE with fixed snow density of 150 kg m⁻³. This density is slightly high for freshly fallen snow in order to compensate for the density increasing effects of wind and grain aging over the storm period. The small accumulations at the NER site limit the effect of any errors introduced by the density estimation. The storm snow totals from the SWR and NER sites were divided by the snow total at the GR site to establish accumulation ratios (ARs) for each storm by site. Snow events were defined as follows:

- (1) Total storm undercatch-corrected precipitation [40] at the GR site greater than 7.0 mm. The 7.0 mm threshold was used to increase the signal-to-noise ratio.
- (2) Mean storm dew point temperature less than -2.0 °C. This is a conservative threshold and though some storms may have been missed, this provided greater confidence in the segregation of snow events.
- (3) The end of a storm event was defined by two consecutive hours without precipitation at the GR site.

In the second step in developing the snow distribution algorithm, accumulations in enhanced deposition zones were addressed. Slope breaks with sufficient upwind exposure produce flow separation and a downwind lee eddy zone with relatively low wind speeds and accentuated accumulations. Winstral and Marks [5] used a time-series of aerial photographs to determine that a 60 m separation distance (i.e. the d_{max} value for the local S_x determinations and the start point for the outlying S_x determinations) and a 5° threshold value of \bar{S}_b for defining drift zones best matched the spatial pattern of observed drifts in Reynolds Mountain East. Winstral and Marks [5] used the ratio of shielded catch at the moderately exposed SWR site to undercatch-corrected precipitation at the sheltered GR site to characterize how much of a factor redistribution was during a given storm period. The greater

the difference between the two sites, the greater the role of redistribution in the simulation. The ratio was used to modulate a drift factor that delivered a multiple of GR site accumulation to the \bar{S}_b -delineated drifts. The multiple varied between 1.0 and 3.5. The upper ends of the ranges were loosely based on observations, prior work in a nearby catchment [3,36,39], and aerial photographs depicting meltout patterns.

Since data from exposed sites are rarely available, simulated intra-storm winds at a hypothetical exposed site were used to modulate the multiple of GR site accumulation delivered to drift-defined cells. The hypothetical exposed site was situated on totally flat terrain (i.e. $\bar{S}_x = 0$). Winds at this site were simulated from wind and \bar{S}_x observations at the SWR site using the methods of Winstral et al. [32]. Storm periods were defined as precipitation occurring in at least one of each two consecutive hours. A dew point temperature threshold of +0.5 °C was established to discern snowfall hours from rainfall hours [55]. If the dew point temperature exceeded this threshold during the storm period those winds were not considered to be a contributing factor to snow accumulation heterogeneity. Storm-averaged wind speeds at this synthetic site were termed FLATU. FLATU was used to calibrate a drift accumulation ratio (DAR) that delivered a multiple of GR site accumulation to all \bar{S}_b -defined drift zones.

The calibration of DAR was based on optimizing a fit of simulated SWE to drift data from the four snow surveys. In order to account for the cumulative weather effects prior to the snow surveys, *Isnobal* was initialized at the start of each snow season. The precipitation forcings for *Isnobal* consisted of "effective precipitation", which included the effects of wind on snow distribution. Multiple model runs were performed to calibrate DAR to snow observations at enhanced deposition sites using FLATU to modulate DAR.

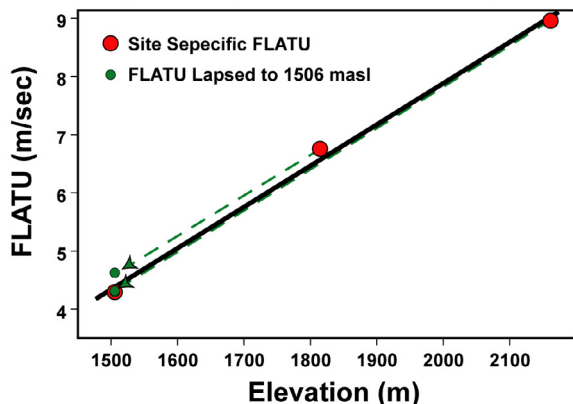
Once the protocols for distributing effective precipitations were established, *Isnobal*-simulated snow distributions were evaluated. *Isnobal* simulations were conducted with two sets of precipitation forcings: the wind-affected precipitation totals established in this work and with precipitation forcings that did not account for wind-affected snow accumulations. Catchment precipitation volumes were the same in each scenario. All other forcings were the same for each scenario. Wind-affected precipitation forcings at Reynolds Mountain East and Upper Sheep Creek were as described above. Wind speeds at Reynolds Mountain East and Upper Sheep Creek were distributed using the procedures described by Winstral et al. [32] and wind data from the SWR site at Reynolds Mountain East and the ME site at Upper Sheep Creek. Residual wind fields based on differences between simulated and observed winds at the remaining sites were distributed over the area based on \bar{S}_x and added back to the simulations to produce the most accurate wind fields possible. The Dobson Creek precipitation and wind forcings required elevation components that are further described below. The *Isnobal* simulations and the procedures applied for deriving all of the other model forcings (solar and thermal radiation, air temperature, vapor pressure, soil temperature) were identical to those described by Winstral and Marks [5] where further details can be found.

The methodologies for distributing the point measurements of wind and precipitation over Dobson Creek had similar frameworks. First, account for any exposure differences amongst the three observation points by lapsing observations to a common exposure. Once the effects of dissimilar exposures at the measurement sites were removed, elevation effects could be determined. Elevation lapse rates were determined and the exposure-equivalent values were lapsed to a common elevation. At this point, the effects of wind exposure and elevation have been removed from the data gathered at each of the three stations. These values were distributed to all pixels in the modeling domain using inverse-distance

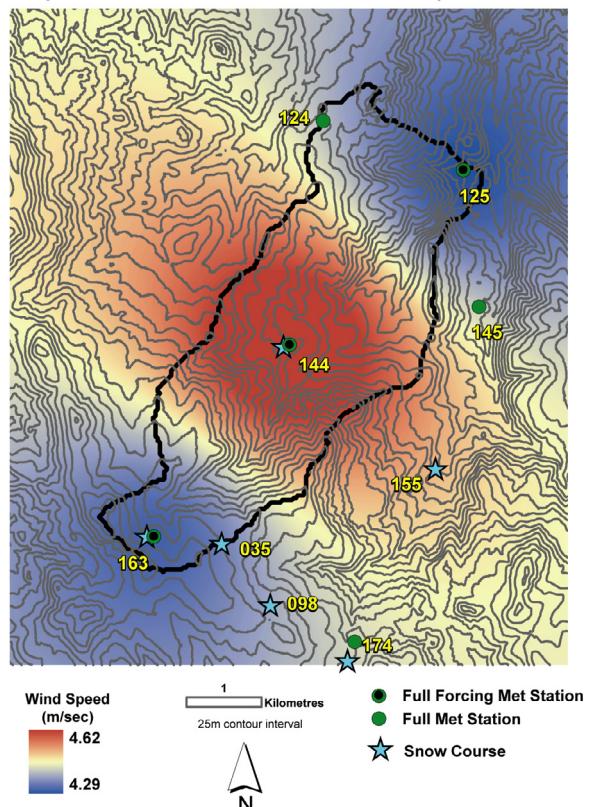
Step 1. Observations lapsed to common exposure (FLATU) and then to common elevation (1506 masl)

	Site 125	Site 144	Site 163
Elevation (m)	1506	1815	2162
Observed Wind Direction	219°	236°	232°
Observed Wind Speed (m/sec)	2.8	5.0	3.9
\bar{Sx}^*	8.08	4.70	16.35
FLATU	4.29	6.75	8.95
FLATU lapsed to 1506 masl	4.29	4.62	4.31

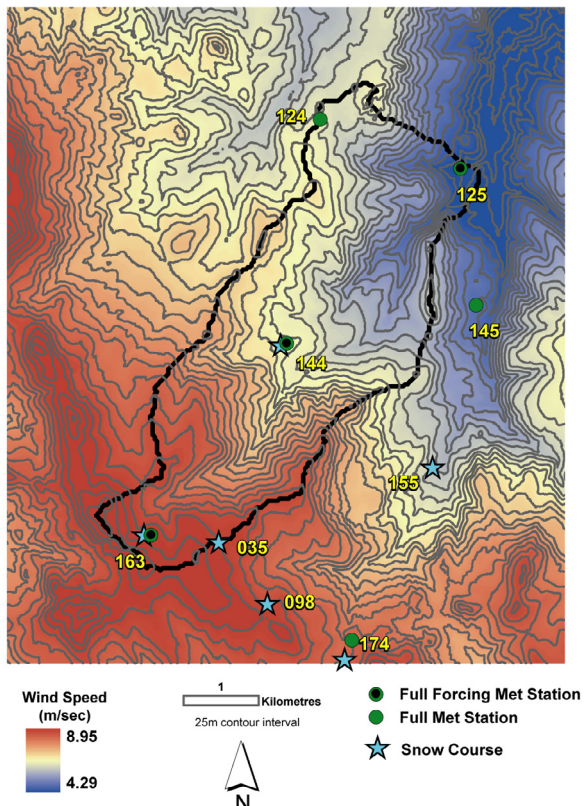
Step 1b. Depiction of elevation lapse rate



Step 2. Distribution of elevation-lapsed FLATU



Step 3. Elevation effects added back in



Step 4. Exposure and canopy effects added back in

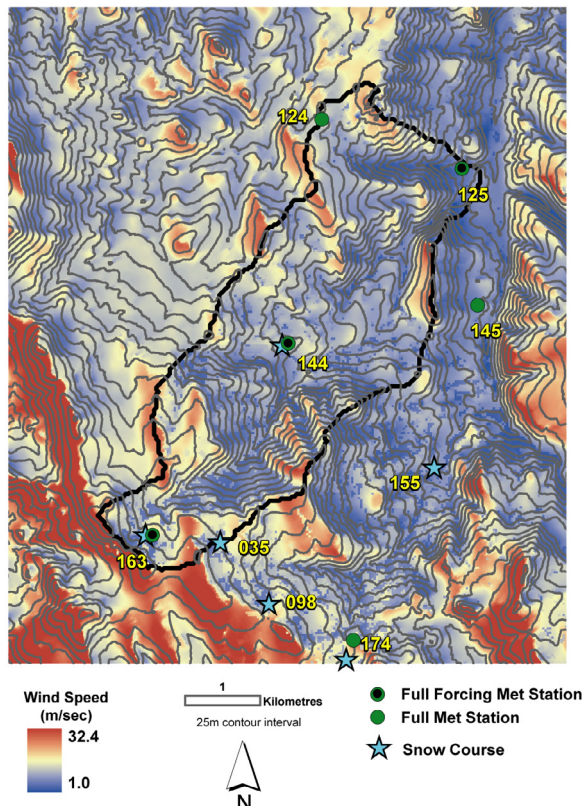


Fig. 4. Example of procedural steps to derive distributed wind speeds. Site specific \bar{Sx}^* values are determined from the observed wind directions to lapse the observations to a common exposure (FLATU) (Step 1). An elevation lapse rate is fit to the FLATU values and the FLATU values are lapsed to the elevation of Site 125 (Step 1b). The exposure and elevation lapsed wind speeds are distributed using an inverse-distance-squared weighting (Step 2). The elevation lapse rate from Step 1b is added back (Step 3) and finally exposures are added back from each pixel's \bar{Sx}^* based on the hourly distributed wind directions (not shown) and Eqs. (3.5) and (3.6) (Step 4).

squared weighting. Lastly, elevation and exposure effects were added back at each pixel from the established lapse rates and terrain/canopy-based distribution techniques to produce distributed forcing fields. This process produced surfaces with site observations preserved and distributed values spatially tied to observations. Specific details on the wind and precipitation distribution methods are presented in the following paragraphs.

The procedure for distributing wind speeds and developing hourly wind fields over Dobson Creek is depicted in Fig. 4. (Note: The precipitation distribution steps represent a subset of the wind steps hence the wind procedure demonstration). Hourly observed wind speeds and wind directions were used to determine \bar{Sx}^* values (i.e. vegetation-compensated \bar{Sx} , see [32]) and observations were lapsed to a common exposure, chosen as $Sx^* = 0.0^\circ$ (termed FLATU) using the methods of Winstral et al. [32] (Step 1 in Fig. 4). A linear least squares fit between elevation and FLATU was then fit to the hourly data (Step 1b in Fig. 4). Since the exposure compensated values were estimates and not absolute measures, all three sites were included to determine a general lapse rate over the entire catchment. The slope of the fitted trend line was used to lapse the FLATU winds to a common elevation chosen as the elevation of the lowest observation (1506 masl). The three FLATU winds at 1506 masl were distributed using inverse-distance squared weighting (Step 2 in Fig. 4). The hourly elevation effect was added back in using the slope of the fitted elevation lapse rate with stipulations that cut the lapse rate off for elevations that exceeded the range of the measured elevations (Step 3 in Fig. 4). Once elevation was added back, only differing exposures needed to be considered. In order to do so, wind directions were distributed so that appropriate \bar{Sx} values could be retrieved from established libraries. Given the broad spatial coverage of the observations and the lack of substantial wind steering terrain in Dobson Creek, observed wind directions were simply distributed using inverse-distance squared weighting (not depicted). Exposure effects, both topographic and vegetative, were then added back to the FLATU values based on Winstral et al. [32]. Two final stipulations stated: (a) winds must exceed 0.447 m s^{-1} and (b) winds must be less than 4.21 times the simulated FLATU (Step 4 of Fig. 4). The minimum value coincides with the anemometer's threshold for movement while also assuring convergence of the turbulent exchange calculations in Isnobal. The maximum value was based on the flexion point of the wind factor- ΔSx^* relationship presented in Eq. (6) of [32].

The three meteorological sites each had co-located unshielded and alter-shielded precipitation gauges. The dual-gauge wind correction formula [40] corrects for wind-induced precipitation undercatch based on the catch ratio at these two gauges. The corrected data represents how much precipitation would have accumulated in a windless environment thus correcting for any between-site exposure differences. The corrected precipitation data were linearly fit with elevation between sites to produce an image akin to that depicted for the wind data in Step 3 of Fig. 4. Each pixel now had a value that represented how much snow would have accumulated at that elevation without the influence of wind. In the final step of the precipitation distribution, wind effects on snow accumulation were accounted for using the procedures developed at Reynolds Mountain East (Section 4.1). In the Reynolds Mountain East and Upper Sheep Creek applications snow accumulations at drift sites were determined from storm-averaged FLATU, which remained spatially consistent throughout the modeling domain – a reasonable assumption in these smaller catchments. In the larger Dobson Creek application, FLATU was determined at each pixel and averaged over storm periods to adjust drift-accumulation-ratios (DARs) at delineated drift locations.

4. Results and discussion

4.1. Reynolds Mountain East: model development and application

4.1.1. Snow-inhibited regions

Determination of accumulation-optimized $dmax$ and $height$ values for use in the \bar{Sx} calculations was based on matching derived \bar{Sx} images to measured SWE distributions. The measured SWE distributions consisted of the survey data inverse distance weighted to a 10 m grid to coincide with the model scale used in this work. The gridded maps indicated a rather consistent trend of snow distribution in all four surveys. In spite of a more than twofold increase in mean SWE from WY2005 to WY2006, the spatial patterns of relative SWE exhibited strong similarities. The April 2006 survey data is shown in Fig. 7. Areas with below average SWE that were focused on in formulating an accumulation-optimized Sx parameter are labeled A, B, and C in Fig. 5. SWE was lowest at A and followed an upward trend through C.

Correlations of \bar{Sx} , derived with varying $dmax$ and $height$, to measured SWE ratios (site SWE divided by GR site SWE) at snow-inhibited sites for the two February snow surveys is presented in Table 1. (Note: SWE ratios described accumulation differences integrated over many storms whereas the previously described accumulation ratios (ARs) refer to distinct storms.) The top-performing were tightly grouped around $R = 0.59$. \bar{Sx} had a greater sensitivity to the $height$ parameter as $dmax$ increased. Four of the highest correlated derivations across the range of $dmax$ are depicted in Fig. 5 to demonstrate the effects of $dmax$ and $height$. Increasing the $dmax$ value limited the terrain deemed highly exposed at A. On this windward facing slope, the lowest \bar{Sx} values (i.e. most exposed) occur when $dmax$ is less than the distance to the streambed. When $dmax$ exceeds a pixel's upwind distance from the streambed, the higher terrain located across the streambed starts to factor into the calculation. Conversely, concurrent increases in $dmax$ and $height$ tended to increase the relative exposure of slopes located near the edge of the catchment such as B and C. Increasing $heights$ reduced the influence of small proximal features on \bar{Sx} allowing increases in $dmax$ to take into consideration more of the generally down-sloping terrain upwind of the catchment boundary. Increasing $heights$ also acted to smooth values across the grid.

It was important that the accumulation-optimized \bar{Sx} distinguish the differing snow-inhibited accumulations and accurately depict their spatial extents. The 300 and 400 m $dmax$ derivations reduced the extent of exposed terrain downslope of A and differentiation between the A and B scour zones was slight, which contrasted observations (Fig. 7). The 100 m $dmax$ derivations provided the greatest differentiation between the A and B scour zones, but the depiction of the A scour zone was extended and the C zone had a good degree of shelter. The 200 m $dmax$ derivations aptly described the extent of the A scour zone, however differences between A and B were less than observed in the 100 m derivation. The 150 m $dmax$ derivation with $height = 3 \text{ m}$ ($R = 0.60$) defined an adequate middle ground between the strengths and weaknesses of the aforementioned derivations and was chosen for the \bar{Sx} derivations that follow. As can be seen in the correlation results, these choices were not absolute and similar results were achievable with other configurations.

In the two-year period there were 30 storms that met the outlined storm criteria. Storm snow totals from the SWR and NER sites were divided by the snow total at the GR site to establish accumulation ratios (ARs). Summary data for these storms are presented in Table 2. ARs and wind speeds by site are plotted in Fig. 6. Fig. 6 clearly suggests that rather than horizontal wind speeds controlling snow accumulations at these sites, it appears that each site has a characteristic AR. The ratios were regressed on mean storm

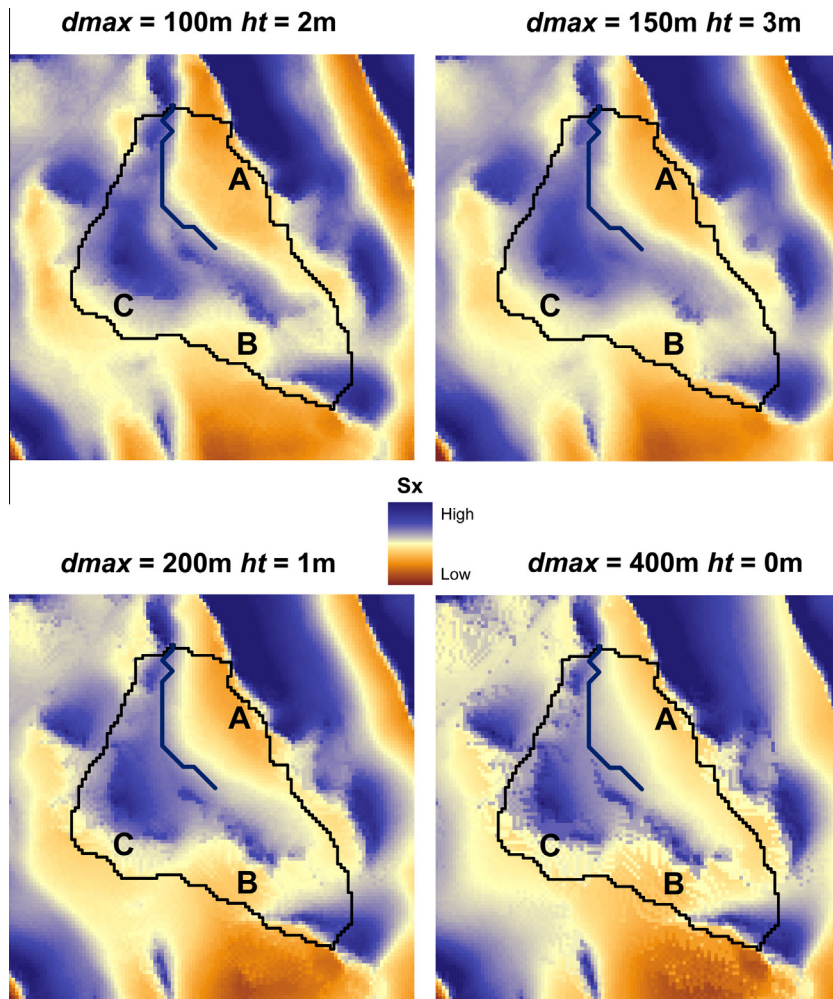


Fig. 5. The sensitivity of \bar{Sx} derivations to the $dmax$ and *height* (*ht*) variables. Derivations are for the prevailing storm direction of 225° . High \bar{Sx} values are indicative of greater shelter. The three scour zones increase in relative accumulations from A through C. Increasing values of $dmax$ decreased the upwind extent of A, increased its crosswind extent, and depicted B as more exposed than A. Increasing height smoothed the effect of small terrain perturbations. The $dmax = 150$ m, *ht* = 3 m derivation retained many of the key features present in the observed snow distribution at accumulation-inhibited sites (reference Fig. 7).

Table 1

Correlation coefficients (R) between \bar{Sx} and accumulation-inhibited February snow accumulations for varying $dmax$ and *height* averaged over SS-2005 and SS-2006.

$n = 4141$		$dmax$ (m)						
height (m)		100	150	200	250	300	350	400
0		0.55	0.575	0.595	0.605	0.605	0.595	0.565
1		0.575	0.6	0.615	0.6	0.575	0.55	0.5
2		0.595	0.6	0.59	0.56	0.525	0.48	0.405
3		0.59	0.595	0.57	0.505	0.445	0.385	0.3
4		0.585	0.59	0.56	0.49	0.41	0.33	0.24

Table 2

Summary of the 30 snow events used to develop the snow-inhibited portion of the snow accumulation algorithm.

	GR site	SWR site	NER site
Total SWE accumulation (mm)	549	292	36
Accumulation ratio	1.0	0.53	0.08
Mean wind speed ($m s^{-1}$)	1.9	7.0	8.9

wind speed and the \bar{Sx} terrain factor associated with the prevailing wind direction for the storm period. Regression results found that Sx was a significant indicator of snow accumulations (Table 3). Wind speed, though significant as a single predictor of AR ($p = 0.0007$, $R^2 = 0.18$), could only account for a small amount of

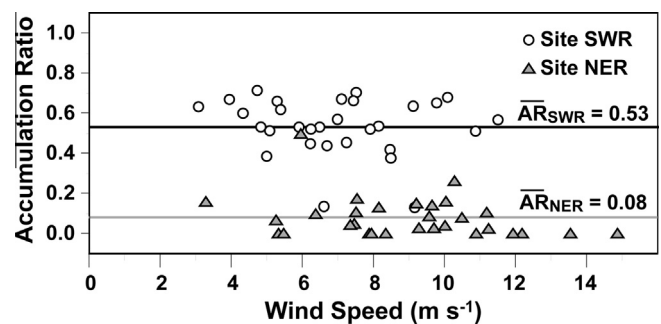


Fig. 6. Accumulation ratio (AR) versus average wind speed for 30 storms during the 2005 and 2006 snow seasons at the two scour sites. Ratio is accumulation at the site divided by accumulation at the sheltered GR site. Both sites seemed to have characteristic ARs that were unaffected by mean storm wind speeds.

the variability in AR ($p = 0.054$) after accounting for the effects of \bar{Sx} in the two-variable regression model. The combination of the two predictors yielded an R^2 value of 0.33, which was higher than the previously mentioned single-variable wind model and a single-variable Sx model ($R^2 = 0.29$). Some of the statistical importance of Sx may be attributable to inter-site differences in Sx . The ability of \bar{Sx} to split the dataset by site corresponds to the overriding inter-

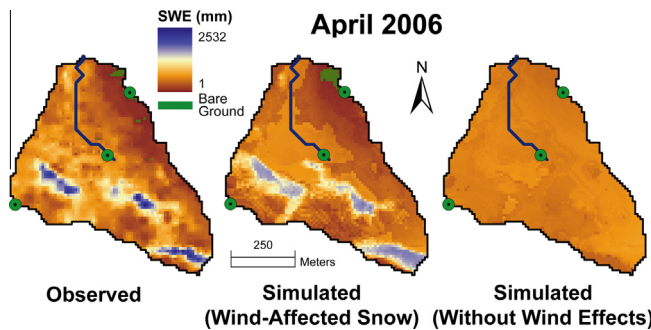


Fig. 7. Comparison of measured and modeled SWE at RME in April-2006. The simulation forced with the presented snow distribution algorithm accurately portrayed the observed heterogeneity from scoured ridges to deep drifts. The simulated drifts were smoother and occupied a slightly larger area than the actual drifts. A simulation forced with spatially distributed energy inputs, but spatially homogenous precipitation fields could not replicate the observed heterogeneity.

Table 3

Results from accumulation ratio (AR) regressed on \bar{Sx} and mean storm wind speed at the meteorological sites ($AR = \beta_0 + \beta_1 \bar{Sx} + \beta_2 \bar{u}$).

n = 60	β	p	R^2
Intercept	0.732	<0.0001	
\bar{Sx}	0.047	0.0007	
$\bar{u} (\text{m s}^{-1})$	-0.024	0.0541	

site AR differences found in Fig. 6. As such, an argument can be made that the statistical significance of \bar{Sx} stems from the fact that ARs and \bar{Sx} have between-site differences that may or may not correspond to a process-dependency. However, \bar{Sx} was correlated to snow distributions (Table 1) and distinguishes the steeper down-slopes at site NER that were statistically linked with lower accumulations ($\beta > 0$). Corresponding with the theory of inhomogeneous precipitation, steeper slopes are capable of increasing turbulence and updrafts that decrease accumulations.

The lack of a strong correlation between wind speeds and storm accumulations was unexpected prompting further investigation. In a regression analysis of intra-site effects, it was found that wind speed was not related to AR at either site ($p = 0.46$ at SWR; $p = 0.12$ at NER). Recalling that shielded gauge catch was applied as the measure of snow accumulation at site SWR in the preceding analysis, two additional measures of SWR:GR accumulation ratios were formulated to test whether this assumption affected results. The ratio of measured storm depths at each site regressed on wind ($p = 1.0$) and the ratio of SWE at site SWR (measured depths converted to SWE using a fixed density) to site GR precipitation regressed on wind ($p = 0.31$) yielded similar results. This confirmed what was apparent in Fig. 6 – each site seems to have a characteristic AR that, at least for the observed temperatures and wind speeds, is not affected by storm-averaged horizontal wind speeds. It is quite possible that wind gusts rather than mean storm wind speeds, as well as vertical wind currents – a generating mechanism of inhomogeneous precipitation – exhibit greater controls on these accumulation differences. The presented data point out the need for further analysis of these influences.

Given the limited evidence that storm-averaged wind speeds affected snow accumulation, wind speeds were not used in the presented model structure for simulating reduced snow accumulations. The model was based solely on the relationship of \bar{Sx} to the snow survey data described earlier and presented in Figs. 5 and 7. A third-order polynomial was fit between \bar{Sx} and the observed SWE fractions (observed SWE divided by GR site SWE) at sites with SWE less than or equal to GR site SWE to define

Table 4

Results of February 2005 and 2006 survey-determined SWE ratios (SR) at snow-inhibited locations regressed on \bar{Sx} ($SR = \beta_0 + \beta_1 \bar{Sx} + \beta_2 \bar{Sx}^2 + \beta_3 \bar{Sx}^3$).

n = 4141	β	p	R^2
Intercept	0.5929	<0.0001	
\bar{Sx}	0.0327	<0.0001	
\bar{Sx}^2	-0.0025	<0.0001	
\bar{Sx}^3	0.0002	<0.0001	

the accumulation-inhibited portion of the snow accumulation algorithm (Table 4):

$$AR = 0.5929 + 0.0327 \bar{Sx} - 0.0025 \bar{Sx}^2 + 0.0002 \bar{Sx}^3 \quad (1)$$

where AR = accumulation ratio (site accumulation/sheltered accumulation) and $\bar{Sx} = \bar{Sx}$ parameter measured on a 10 m grid with $dmax = 150$ m, $height = 3$ m

In application, AR was limited to a range of 0.0–1.0. Though all the terms were significant in Eq. (1), there was considerable scatter of observations around the fitted relationship. Radiative and turbulent fluxes, which can substantially affect SWE, were not considered and may explain some of the scatter. Natural, small-scale variability occurring at subpixel length scales can be large in this region and would also contribute to scatter. It must also be recognized that an extremely complex process has been greatly simplified and parameterized in order to capture hydrologically relevant snowcover differences in a distributed snow model. The true test of Eq. (1) will be the effect it has on the subsequent snow simulations.

The linear model that included \bar{Sx} and wind (Table 3) was also tested with similar results. Due to space limitations, results from the latter application are not presented. The goal of this research was to establish an efficient method for distributing wind-affected snow accumulations from typically available data. Either of these models would fulfill these goals. Horizontal wind speeds are a strong component of snow redistribution models (e.g. [13–15] and others). If and when a stronger relationship between generally available wind speed data and snow accumulations can be established, it can easily be incorporated into the presented modeling framework.

4.1.2. Snow-enhanced regions

In spite of the inability to establish a strong relationship between horizontal wind speeds and decreased snow accumulations, it is well documented that wind speeds affect redistribution, especially drifting ([56–58] and others). While it would have been possible to simply establish a static drift-accumulation-ratio (DAR), linking DAR to wind speeds matched our understanding of the physical processes that govern snow drifting. An upper limit of DAR needed to be determined, as well as the relationship between FLATU and DAR. Without storm-resolved drift accumulation data, the selection of a maximum DAR and the FLATU–DAR relationship presented here is but one possible solution of which there are many. The transport of snow in suspension increases as a power function of wind speed [14], so a similar relationship between FLATU and DAR was sought. Adjustments to the FLATU–DAR relationship and its limits were then made from comparisons of *Isnobal* modeled drift SWE to measured SWE in each of the four snow surveys.

An optimal relationship between FLATU and DAR was found that minimized errors between *Isnobal*-modelled and measured SWE at the drift locations. DAR as a function of FLATU was defined as:

$$DAR = e^{(-0.0956 * FLATU + 0.0289 * FLATU^2)} \quad (2)$$

DAR was limited to a range of 1.1 to 4.2 which equated to FLATUs of 3.8 and 8.9 m s^{-1} respectively.

4.1.3. Spatial simulations

The only precipitation data used to derive the effective precipitation forcing fields, which included the effects of wind on snow accumulations, came from GR site data corrected for wind-induced undercatch [40]. Hourly wind speeds were distributed as described

in the methods section. Storm periods were segregated and event-specific wind data, both speed and direction, were integrated over the period. At the conclusion of each storm period, the mean resultant wind direction and the average wind speed at the hypothetical flat site (FLATU) for the storm period were determined. Once these

Table 5

Additional effects on modeled snow distributions.

Vegetation type	Description	Effect on Accumulation Ratio (AR, Eq. (3.11))
Small sagebrush	Heights less than 50 cm. Much of the area in this classification has very little winter groundcover.	None
Mid sagebrush	Approximate heights of 50–100 cm; spacing on the order of vegetation heights	AR = 1.0 until accumulated snow depth reached 20 cm
Tall sagebrush	Approximate heights of 1–2 m, spacing on the order of vegetation heights.	AR = 1.0 until accumulated snow depth reached 80 cm
Willow	Deciduous, occurring in tight clumps along creek. Approximate heights of 2–3 m.	Terrain determined AR increased by 40% up to a maximum of 1.0
Aspen	Deciduous, approximate heights of 4–8 m, spacing on the order of metres	Terrain determined AR increased by 40% up to a maximum of 1.0
Fir	Approximate heights of 7–10 m with spacing on the order of 5–10 m.	AR = 1.0
In-forest-opening	Sagebrush cell adjacent to at least five cells classified as aspen, willow, or fir	AR = 1.0
Leeslopes: $3^\circ < \overline{Sb} < 5^\circ$ or < 30 m downwind of fir tree	Moderate terrain/vegetation wind shelters downwind of high wind areas with large fetches. Sheltering feature within 200 downwind meters of exposed, high wind area.	AR = 1.5
Leeslope: $0^\circ < \overline{Sb} < 3^\circ$	Small terrain traps triggered by slope breaks within 200 downwind meters of high wind areas.	Terrain determined AR increased by 100% up to a maximum of 1.0

Note: effective sagebrush heights are less than their actual heights since they become progressively thinner with height and compact under the weight of snow.

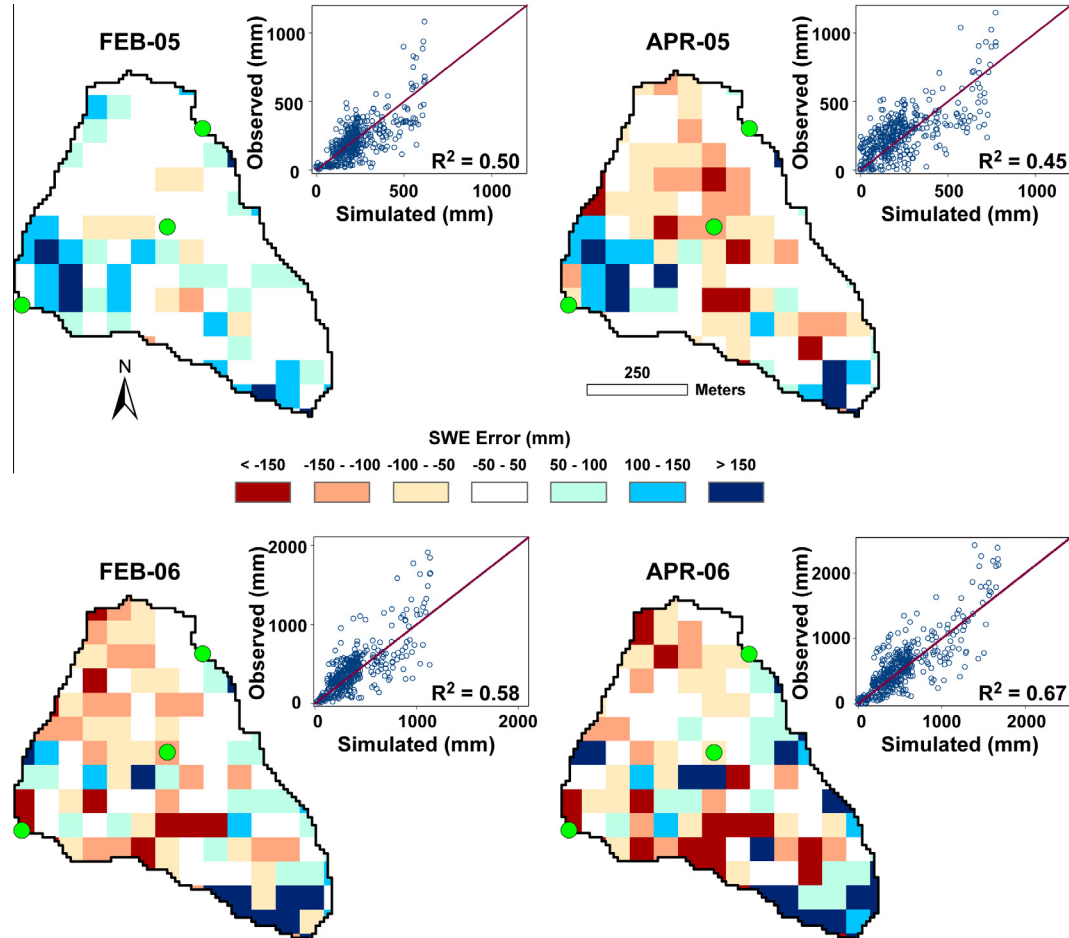


Fig. 8. Scatterplots of simulated and observed SWE along with the spatial distribution of errors coinciding with the four survey dates in SS-2005 and SS-2006 at RME. Errors were averaged over 60 m pixels in the spatial representation. Positive errors are model overestimations. The red line in the scatterplots represents the one-to-one relationship.

storm characteristics were determined, the storm period was stepped through again to distribute hourly precipitation/snow accumulation. Hourly precipitation images were derived from undercatch-corrected hourly precipitation [40] at the GR site, vegetation, \bar{S}_x , and \bar{S}_b . The latter two were referenced by mean resultant wind direction for the storm period.

If the hourly dew point temperature was above 0.5 °C (i.e. rain), it was assumed that snow redistribution and inhomogeneous precipitation were not factors and GR site precipitation was simply assigned to all cells. Hourly dew point temperatures below 0.5 °C indicated that it was snowing and considerations for differential accumulation rates were made. Pixels that were not in a \bar{S}_b -defined drift zone and contained small sagebrush or no vegetation received a fraction of hourly GR precipitation (AR) based on Eq. (1). Taller shrubs and bushes, as observed at SWR (Fig. 2), affect snow accumulations until buried by snow. Based on field observations, AR values were adjusted to account for these effects (Table 5). Pixels in \bar{S}_b -defined drift areas received a multiple of GR precipitation based on Eq. (2). Gentle leeward slopes adjacent to exposed ridge-lines are subject to high snow transport fluxes. Small topographic breaks and sparse trees can produce preferred downwind accumulations in these regions. Enhanced snow accumulations were found under such conditions at Reynolds Mountain East and additional observation-based compensations to AR were made (Table 5).

Isnobal-simulated SWE forced with the distributed precipitation forcings described above did an excellent job of depicting the very heterogeneous snow distributions captured in the snow surveys. Modeled and measured SWE for the April-2006 survey data are presented in Fig. 7. For comparison, *Isnobal* forced with an equal volume of precipitation, but with a homogeneous distribution is also included in Fig. 7. The model capably and efficiently depicted the major features of heterogeneity and did an excellent job predicting distributed SWE values. The simulated field does not fully capture the highest observed drift accumulations nor does it feature the natural small scale variability. The simulated drifts are

smoother and occupy a slightly larger area than the actual drifts. These results are to be expected given the virtual impossibility of capturing the natural small-scale variability with a 10-m model. The improvements garnered from the snow distribution module are readily apparent in comparison to the model that didn't capture these heterogeneities.

Error maps of simulated SWE minus measured SWE are presented in Fig. 8. In these grids, errors were averaged over a 60 m × 60 m area. The averaging reduced the effects of sub-pixel spatial anomalies not considered in the model (e.g. tree wells), measurement errors, the aforementioned scaling differences between observations and simulations, and spatial errors associated with GPS and DEM accuracy. There are some consistent year-to-year errors – over-predictions upwind of the far southeast drift and a general area of under-predictions downstream of the GR site. The latter could be a product of the chosen d_{max} value. In many other instances there is little inter-year error consistency. Year-to-year differences suggest that these errors are random rather than systematic and that potentially a process is not being fully captured by the model. An example of the latter could be the over-predictions northeast of site SWR in the drier SS-2005. The lack of snow may have exposed a greater amount of sagebrush above the snow surface thereby enhancing radiation inputs [59] not accounted for in the model.

R^2 values as a measure of fit between measured and simulated SWE were based on a comparison of 30 m products – the 30 m gridded survey data and simulated SWE averaged over the nine 10 m pixels overlain by the 30 m pixel. *Isnobal* forced with the wind-affected algorithm had R^2 values ranging from 0.50 to 0.67 for the four surveys (scatterplots in Fig. 8). Models forced with the spatially consistent precipitation inputs had R^2 values of less than 0.03. These differences clearly point out that energy balance differences cannot account for the first-order observed heterogeneities. R^2 values for the wind-affected model compare quite favorably to prior regression-based statistical analyses of snow

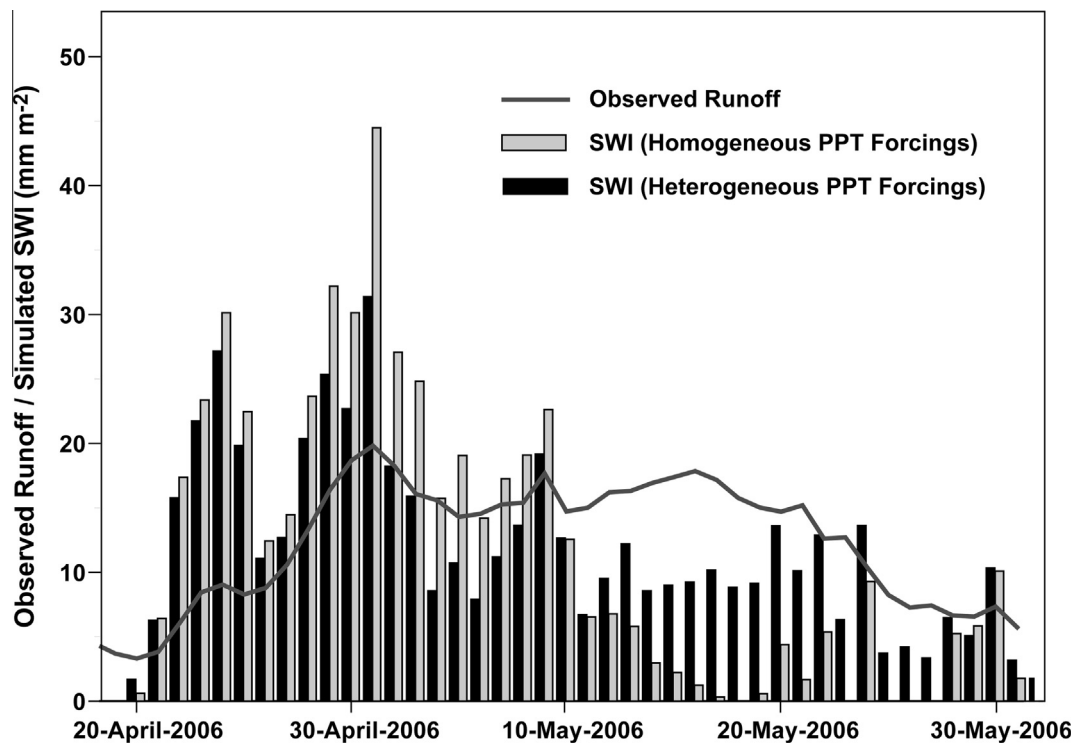


Fig. 9. Daily observed runoff and simulated SWI during spring meltout at Reynolds Mountain East. During the second week of May the simulation forced with spatially homogeneous snow forcings had very little SWE remaining and snowmelt contributions to SWI approached zero. The model forced with the wind-affected snow forcings continued to simulate consistent snowmelt inputs through the third week of May consistent with the steady flow observed during this period.

distribution in mountain environments with average (when more than one model presented) or singular R^2 values of 0.25 ([60]), 0.34 ([31]), 0.37 ([30]), 0.50 ([28]), 0.56 ([61]), and 0.59 ([62]). The predictive capabilities of these regression-based statistical models have yet to be tested whereas the physically-based model pre-

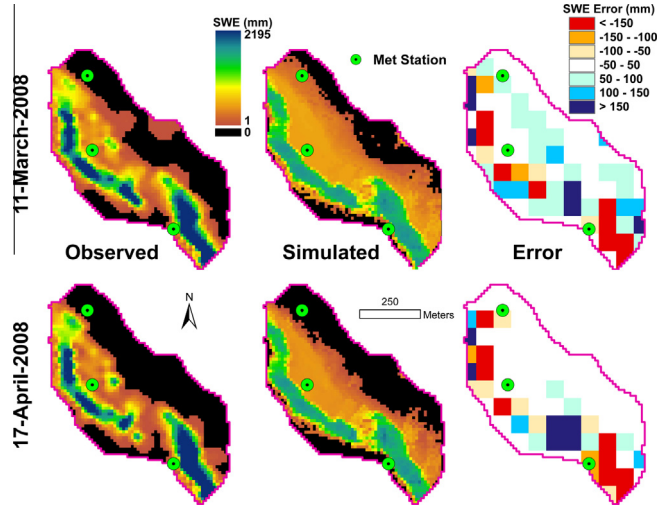


Fig. 10. Results from the Upper Sheep Creek application. The simulated drifts and scour zones were well placed. Simulated drifts had smoother SWE distributions and were spread over a slightly larger area than the actual drifts. Errors were averaged over a $60 \text{ m} \times 60 \text{ m}$ area. The averaging reduced the effects of spatial mismatches between modelled and observed SWE.

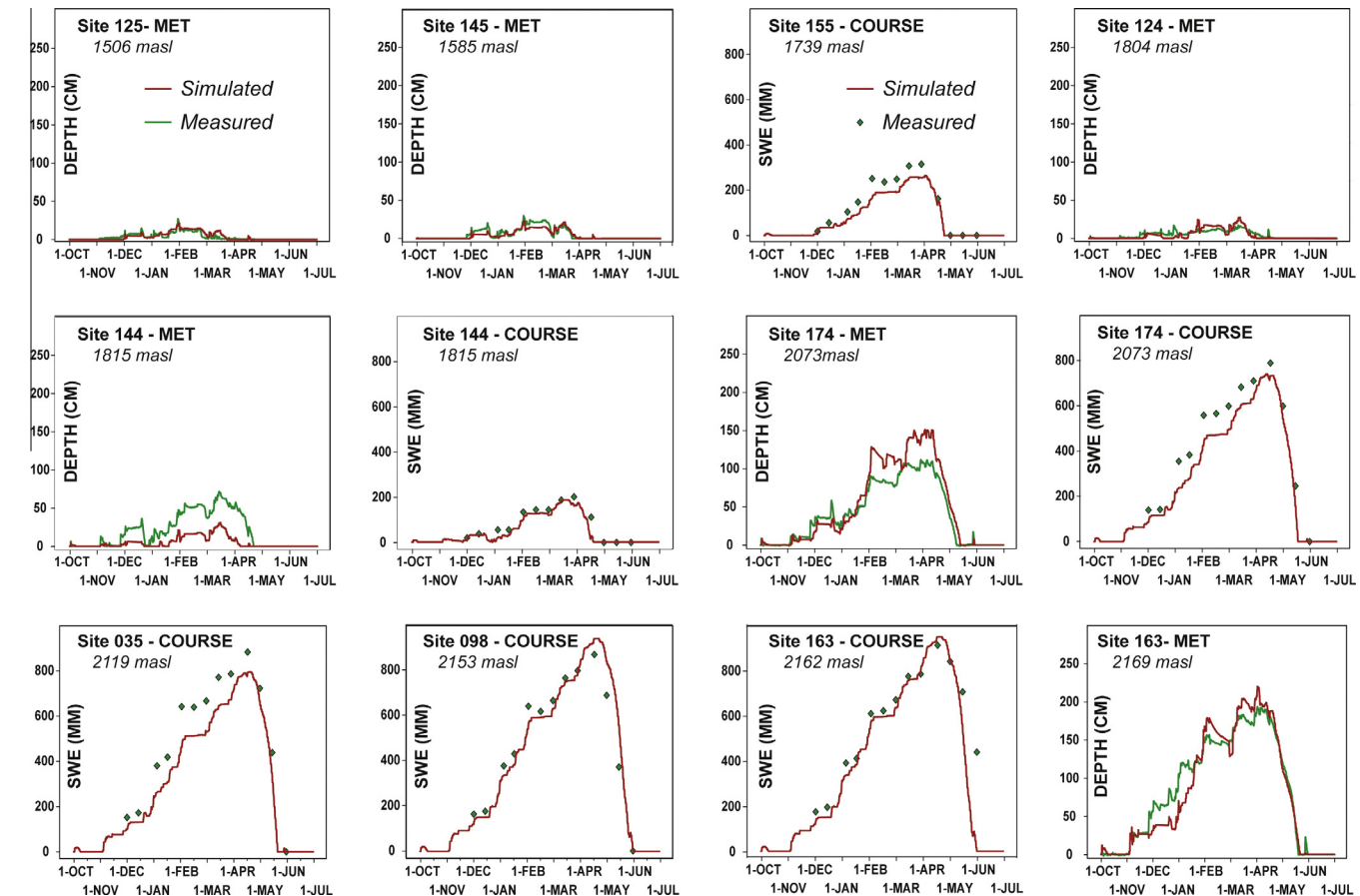


Fig. 11. Simulated and measured snow depths or snow water equivalents at the 12 Dobson Creek validation sites for SS-2006. Site elevations increase from left to right and from the top to bottom.

sented here is ideally suited to this task. Predictive capabilities are tested in the subsequent Upper Sheep Creek application.

The model that included the heterogeneous precipitation inputs also simulated a very different runoff pattern than the model forced with the homogeneous precipitation fields. Differences between the models became evident during the spring snowmelt period and were accentuated in the wetter SS-2006 (Fig. 9). During the period beginning on 28-April-06 through the peak of observed runoff (01-May) and ending on 09-May-06, basin-integrated surface water input (SWI) – snowmelt plus rain falling on either a saturated, 0° snowpack or bare ground – from the homogenous forcings were consistently higher than from the heterogeneous forcings. In the model without wind effects, SWI contributions were similar throughout the basin whereas SWI was reduced in the wind-affected model due to supply limits on exposed slopes and the greater energy demands required to bring the drifted areas to 0°C . Cumulative SWI from the homogeneous model for the 12 day period was 279 mm m^{-2} compared to 198 mm m^{-2} for the distributed model – an increase of 41%. By 12-May nearly all of the homogenous snowpack had melted while the deeper snows continued to contribute to SWI in the heterogeneous model. From 12-May through 26-May, as measured runoff at the weir continued at a steady pace, the homogeneous model produced only 34 mm m^{-2} of SWI – primarily from rainfall – while the heterogeneous model simulated consistent daily snowmelt contributions totaling 135 mm m^{-2} of SWI. In Reynolds Mountain East, where daily SWI and observed streamflow are closely correlated after the initial spring freshet [5], SWI simulated with the homogenous forcings was incapable of supporting mid-May observations.

4.2. Upper Sheep Creek: application

The distributions of simulated wind-affected SWE and measured SWE in Upper Sheep Creek were quite similar (Fig. 10). The model aptly captured the highly heterogeneous snow distribution. The large drifts on the northeast facing slopes along with the snow-bare windswept southwest slopes and ridgelines can be readily seen in the simulations. As was the case in the Reynolds Mountain East simulation the simulated drifts were smoothed over a greater area than the actual drifts. Some of the smaller observed heterogeneities such as those east and north of the LME site were not picked up by the model. These modeling mismatches could be related to differences in model and measurement scales or natural processes not accounted for in the model.

R^2 values for the March and April survey dates, based on 30 m pixel values, were respectively 0.70 and 0.66 for the wind-affected distributions. Corresponding R^2 values for the simulations that did not include wind-affected precipitation forcings were 0.09 and 0.10. These model comparisons again point out the vital impact

of wind on snow distribution in this region. Results for the wind-affected precipitation forcings were in fact better than the results obtained at Reynolds Mountain East and once again compared quite favorably with the previously cited results for regression-based statistical models. These results are even more encouraging in light of the fact they were produced from an independent sample and represent true model skill whereas the earlier reported results were produced using in-sample cross-validation which tends to contain a positive or optimistic bias [63].

The improved snow distribution directly translated to an enhanced depiction of snowmelt. Early snowmelt in Upper Sheep Creek primarily recharges the groundwater [64] and only after sufficient recharge has occurred does continued snowmelt produce a stream response. Meltwater is routed via subsurface flow to the stream channel with response times of 3–5 days [3,36]. In SS-2008, streamflow commenced on 06-May with the rising limb of the hydrograph beginning on 20-May and the runoff peak occurring on 23-May. The simulation forced with the spatially homogeneous precipitation forcings became snow-free on 09-May and only produced 1 mm m^{-2} of SWI during the lead up to increased streamflow (15-May to 20-May). On the other hand, the model forced with the wind-affected precipitation had its highest concentration of seasonal SWI during this period simulating a total 63 mm m^{-2} SWI.

Table 6

Summary statistics for simulated snow depth/mass at the 12 Dobson Creek validation sites. RMSE is expressed in cm of depth for the meteorological stations and in mm of SWE at the snow courses. N-S efficiency refers to the Nash–Sutcliffe efficiency coefficient [47]. N-S = 1.0 would indicate an exact match between observations and predictions; N-S < 0 indicates that in terms of variance the mean is a better predictor than the model.

Site	N-S efficiency	RMSE
125-Met	0.66	2.6 cm
145-Met	0.80	3.4 cm
155-Course	0.88	40.6 mm
124-Met	0.32	3.9 cm
144-Met	0.05	21.5 cm
144-Course	0.81	30.6 mm
174-Met	0.76	19.1 cm
174-Course	0.89	81.8 mm
035-Course	0.84	107 mm
098-Course	0.92	72.90 mm
163-Course (w/o mid-melt point*)	0.65 (0.94)	134.5 mm (57.7 mm)
163-Met	0.93	18.0 cm

* 163-Course statistics with 01-June-2006 point removed.

4.3. Dobson Creek: application

The point comparisons of modeled and measured snow at the twelve observation sites produced Nash–Sutcliffe (N-S) efficiency coefficients [65] that were above 0.80 at many of the sites (Fig. 11, Table 6). Though data on intra-elevation wind effects were limited in these point observations, it can be seen that the model aptly captured the considerable effect elevation has on snow accumulation and melt in this catchment. Melt events occurred throughout the winter at the low elevation sites producing a thin and often ephemeral snow cover. The high elevation sites continued to accumulate snow throughout the winter before reaching peaks in late April and undergoing a rapid melt out. These patterns were well captured by the model. The model did well differentiat-

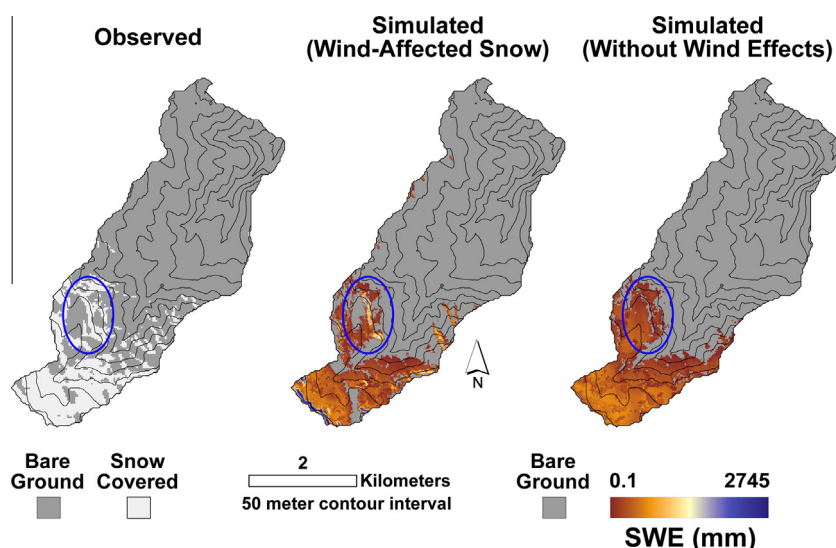


Fig. 12. Simulated SWE and observed snow-covered-area (SCA) on 10-May-2006 in Dobson Creek. The pattern of snow-covered and snow-free areas in the upper basin was simulated very well by the wind-affected accumulation model. The errors of commission on the north-facing slopes along the southern boundary may be due to the inability of the Landsat TM imagery to discern the snow beneath the dense fir trees on these slopes (see Fig. 1). The highlighted region contains a wind-swept ridge and adjacent lee-slope drift. The wind-affected model accurately captured this pattern whereas the model without wind-affected accumulations placed more snow on the ridge and little to no snow in the drift area.

ing between Site 124 and the Site 144 snow course, which have similar elevations but different exposures. The lowest N-S efficiency score occurred at the Site 144 met station though the model performed quite well at the adjacent snow course. Though the two sites had similar snow-covers, \bar{S}_x values were slightly lower (greater exposure) at the met site creating the modeled disparity. The simulated melt rate at the Site 163 snow course was greater than the observed melt rate. Dense fir trees just south of this site provide solar shading to much of the snow course. These trees are mapped in adjacent pixels creating a boundary effect not accounted for in the radiation model. N-S scores at this site are reported with and without the influential melt season data point.

The Landsat TM image was captured on 10-May-2006 approximately two weeks after peak accumulation at the upper elevation snow courses (see Fig. 11). The processed image displays the locations of drifts, late-lying snow, and areas that have completely melted out and provided some insight into the spatial validity of the simulated snow distribution. On this date the higher elevations maintained a nearly continuous snow cover that concealed much of the SWE heterogeneity known to exist in this region. Mid/high elevations were exhibiting the effects of differential snow accumulations while the lower catchment was snow-free. Fig. 12 indicates that there was excellent agreement between simulated and observed snow-covered-area (SCA) on this date. Respective SCA depictions in the simulation and imagery were 19% and 18%. The lack of snow in the lower basin is readily apparent in both the model and observations. The mosaic of snow-covered and snow-free areas attributable to wind effects in the upper basin was remarkably well represented in the model. Some errors of commission (i.e. model-predicted snow with no observed snow) on the north-facing slopes may be due to the inability of the Landsat sensor to discern snow beneath the dense fir trees on these slopes (Fig. 1). Once more, the simulation that did not include wind-affected snow accumulations depicted a more homogeneous SWE distribution. The highlighted region in Fig. 12 shows an exposed ridge with very little snow on it and a lee-slope drift zone. This scoured ridge and drift are prominent features observed in many satellite observations that were well depicted in the wind-affected model. When wind effects on accumulation rates were not accounted for, modeled SWE was greater on the higher elevation wind-swept ridge than in the slightly lower drift area where little to no snow remained in the simulation.

5. Conclusions

An efficient snow distribution algorithm that accounts for differential wind-affected accumulations due to the processes of inhomogeneous precipitation and redistribution of snow by wind was developed and successfully applied in three catchments. The algorithm, based on terrain structure with modifications for vegetation cover, accurately portrayed the disparate snow distribution from scoured ridges to deep drifts in both wet and dry seasons using precipitation data solely from wind-sheltered stations. Simulated SWE distributions from a physically-based distributed snow model forced with the developed algorithm were far more accurate than simulations that lacked a wind-affected accumulation component. Additionally, it was shown that simulated surface water inputs from the wind-affected snow simulations corresponded with observed springtime runoff patterns in situations where a model that did not account for wind effects could not. R^2 values matching simulated and observed SWE distributions equaled or bettered published cross-validation results from complex regression-based snow distribution modeling done in similar environments.

The Dobson Creek simulation demonstrated that the design and structure of this model is appropriate for applications over larger areas in operationally-realistic settings where data is limited. Distributed hourly forcings were established over a 6.67×10^5 pixel grid from typically-collected mountain weather data, a digital elevation model (DEM), and commonly available vegetation data. While observed precipitation lapse rates were available to capture the effects of elevation on precipitation in this application, others have shown how long-term data can be used to estimate lapse rates for these purposes when observations are spatially limited (e.g. [27,66–69]). Forcing data for the model need not be limited to observations; downscaled numerical weather prediction products, or radar retrievals could just as easily be used to describe elevation gradients with the snow distribution algorithm handling intra-elevation wind-induced accumulation differences.

Spurred by these initial results, ongoing research will seek to further improve the distribution techniques. As presented, the algorithm for distributing snow to accumulation-inhibited sites is based solely on terrain and vegetation structure. Though upwind terrain structure plays an important role in affecting snow accumulations, it is quite likely that wind speed and air temperature [23,57] also play roles. The data in this research however, were unable to substantiate any of these latter trends. Future research into wind and temperature dependencies will help to refine the current algorithm. Recently developed technologies such as ground-based LiDAR [7,9] and active radar [70,71] systems are capturing storm specific accumulation patterns that can further improve the distribution algorithm, particularly in accumulation-enhanced regions.

Acknowledgments

The authors would like to thank Tobias Jonas, Rebecca Mott, and an anonymous reviewer for their insightful reviews of this paper. We would also like to thank Mark Murdock, Jim Windom, John Wilford, Steven Van Vactor and the rest of the folks that helped to collect and archive the presented data. The data and analysis presented in this paper were funded in part by USDA-ARS CRIS *Understanding Snow and Hydrologic Processes in Mountainous Terrain with a Changing Climate* (5362-13610-008-00D), USDA-ARS Headquarters Student Career Experience Program (SCEP), USDA-NRCS Conservation Effects Assessment Project (5352-13610-009-14R), USDA-NRCS Water and Climate Center-Portland, Oregon (5362-13610-008-03R), NSF-CBET (0854553), NSF-MRI (EAR-1126887) and NSF Idaho EPSCoR Program (EPS-0814387). Any reference to specific equipment types or manufacturers is for information purposes and does not represent a product endorsement or recommendation. USDA is an equal opportunity provider and employer.

References

- [1] Tarboton DG, Al-adhami MJ, Bowles DS. Preliminary comparisons of snowmelt models for erosion prediction. In: Proceedings of Western Snow Conference, 1991, pp. 79–90.
- [2] Williams MW, Melack JM. Effects of spatial and temporal variation in snow melt on nitrate and sulfate pulses in melt waters within an alpine basin. Ann Glaciol 1989;13:285–9.
- [3] Luce CH, Tarboton DG, Cooley KR. The influence of the spatial distribution of snow on basin-averaged snowmelt. Hydrol Process 1998;12:1671–83.
- [4] Brooks PD, Williams MW. Snowpack controls on nitrogen cycling and export in seasonally snow-covered catchments. Hydrol Process 1999;13:2177–90.
- [5] Winstral A, Marks D. Simulating wind fields and snow redistribution using terrain-based parameters to model snow accumulation and melt over a semi-arid mountain catchment. Hydrol Process 2002;163:585–603.
- [6] Seyfried S, Grant LE, Marks D, Winstral A, McNamara J. Simulated soil water storage effects on streamflow generation in a mountainous snowmelt environment, Idaho, USA. Hydrol Process 2009;23:858–73.
- [7] Schirmer M, Wirz V, Clifton A, Lehning M. Persistence in intra-annual snow depth distribution Part 1: Measurements and topographic control. Water Resour Res 2011;47:W09516.

- [8] Mott R, Bavay M, Grünwald T, Lehning M. Understanding snow-transport processes shaping the mountain snow-cover. *Cryosphere*. 2010;4:545–559.
- [9] Egli L, Jonas T, Grünwald T, Schirmer M, Burlando P. Dynamics of snow ablation in a small Alpine catchment observed by repeated terrestrial laser scans. *Hydrol Process* 2012;26:1574–85.
- [10] Greene EM, Liston GE, Pielke RA. Simulation of above treeline snowdrift formation using a numerical snow-transport model. *Cold Regions Sci Technol* 1999;30:135–44.
- [11] Daly SF, Davis RE, Ochs E, Pangburn T. An approach to spatially distributed snow modelling of the Sacramento and San Joaquin basins, California. *Hydrol Process* 2000;14:3257–71.
- [12] Lehning M, Löwe H, Ryser M, Raderschall N. Inhomogeneous precipitation distribution and snow transport in steep terrain. *Water Resour Res* 2008;44:W07404.
- [13] Pomeroy JW, Gray DM, Landine PG. The Prairie blowing snow model: characteristics, validation, operation. *J Hydrol* 1993;144:165–92.
- [14] Liston GE, Sturm M. A snow-transport model for complex terrain. *J Glaciol* 1998;44:498–516.
- [15] Dadic R, Mott R, Lehning M, Burlando P. Parameterization for wind-induced preferential deposition of snow. *Hydrol Process* 2010;24:1994–2006.
- [16] Mott R, Schirmer M, Lehning M. Scaling properties of wind and snow depth distribution in an Alpine catchment. *J Geophys Res* 2011;116:D06106.
- [17] Daly C, Neilson RP, Phillips DL. A statistical-topographic model for mapping climatological precipitation over mountainous terrain. *J Appl Meteorol* 1994;33:140–58.
- [18] Garen DC, Johnson GJ, Hanson CL. Mean areal precipitation for daily hydrologic modeling in mountainous regions. *Water Resour Bullet* 1994;30:481–91.
- [19] Thornton PE, Running SW, White MA. Generating surfaces of daily meteorological variables over large regions of complex terrain. *J Hydrol* 1997;190:214–51.
- [20] Essery R, Li L, Pomeroy JW. A distributed model of blowing snow over complex terrain. *Hydrol Process* 1999;13:2423–38.
- [21] Bernhardt M, Zängl G, Liston GE, Strasser U, Mauser W. Using wind fields from a high-resolution atmospheric model for simulating snow dynamics in mountainous terrain. *Hydrol Process* 2009;23:1064–75.
- [22] Bavay M, Lehning M, Jonas T, Löwe H. Simulations of future snow cover and discharge in Alpine headwater catchments. *Hydrol Process* 2009;23:95–108.
- [23] Blöschl G, Kirnbauer R, Gutknecht D. Distributed snowmelt simulations in an alpine catchment 1. Model evaluation on the basis of snow cover patterns. *Water Resour Res* 1991;27:3171–9.
- [24] Cline DW. Modeling the redistribution of snow in alpine areas using geographic information processing techniques, In: Proceedings of the Eastern Snow Conference, 1992, pp. 13–24.
- [25] Lapen DR, Martz LW. The measurement of two simple topographic indices of wind sheltering-exposure from raster digital elevation models. *Comput Geosci* 1993;19:769–79.
- [26] Purves RS, Barton JS, Mackaness WA, Sugden DE. The development of a rule-based spatial model of wind transport and deposition of snow. *Ann Glaciol* 1998;26:197–202.
- [27] Hartman MD, Baron JS, Lammers RB, Cline DW, Band LE, Liston GE, et al. Simulations of snow distribution and hydrology in a mountain basin. *Water Resour Res* 1999;35:1587–603.
- [28] Winstral A, Elder K, Davis RE. Spatial snow modeling of wind-redistributed snow using terrain-based parameters. *J Hydrometeorol* 2002;3:524–38.
- [29] Winstral A. Implementation of digital terrain analysis to capture the effects of wind redistribution in spatial snow modeling [M.S. thesis]. Fort Collins, CO, USA: Colorado State University; 1999.
- [30] Molotch NP, Colee MT, Bales RC, Dozier J. Estimating the spatial distribution of snow water equivalent in an alpine basin using binary regression tree models: the impact of digital elevation data and independent variable selection. *Hydrol Proc* 2005;19:1459–79.
- [31] Erickson TA, Williams MW, Winstral A. Persistence of topographic controls on the spatial distribution of snow in rugged mountain terrain, Colorado, United States. *Water Resour Res* 2005;41:W04014.
- [32] Winstral A, Marks D, Gurney R. An efficient method for distributing wind speeds over heterogeneous terrain. *Hydrol Process* 2009;23:2526–35.
- [33] Marks D, Domingo J, Susong D, Link T, Garen D. A spatially distributed energy balance snowmelt model for application in mountain basins. *Hydrol Process* 1999;12:1569–87.
- [34] Hanson CL. Long-term precipitation database: Reynolds Creek experimental watershed, Idaho United States. *Water Resour Res* 2001;37:2831–4.
- [35] Elder K, Dozier J, Michaelsen J. Snow accumulation and distribution in an alpine watershed. *Water Resour Res* 1991;27:1541–52.
- [36] Flerchinger GN, Cooley KR. A ten-year water balance of a mountainous semiarid watershed. *J Hydrol* 2000;237:86–99.
- [37] Cooley KR. Snowpack variability on western rangeland. In: Proceedings of the Western Snow Conference, 1988, pp. 1–12.
- [38] Tarboton D, Blöschl G, Cooley K, Kirnbauer R, Luce C. Spatial snow cover processes at Kühtai and Reynolds Creek. In: Grayson R, Blöschl G, editors. *Spatial patterns in catchment hydrology: observations and modelling*. United Kingdom: Cambridge University Press; 2000. p. 158–86.
- [39] Prasad R, Tarboton DG, Liston GE, Luce CH, Seyfried MS. Testing a blowing snow model against distributed snow measurements at Upper Sheep Creek, Idaho, United States of America. *Water Resour Res* 2001;37:1341–50.
- [40] Hanson CL, Pierson FB, Johnson GL. Dual-gauge system for measuring precipitation: historical development and use. *J Hydrol Eng* 2004;9:350–9. Accepted for publication.
- [41] Marks D, Winstral A, Reba M, Pomeroy JW, Kumar M. An evaluation of methods for determining during-storm surface precipitation phase and the rain/snow transition elevation at the surface in a mountain basin. *Adv Water Resour* 2013;55:98–110.
- [42] Davis RE, Jordan R, Daly SF, Koenig GG. Validation of snow models. In: Anderson MG, Bates PD, editors. *Model validation: perspectives in hydrological science*. Wiley; 2001. p. 261–92.
- [43] NASA Landsat 7 Science Data Users Handbook. Greenbelt, MD. Available at: http://landsathandbook.gsfc.nasa.gov/pdfs/Landsat7_Handbook.pdf.
- [44] Hall DK, Riggs GA, Salomonson VV. Development of methods for mapping global snow cover using moderate resolution imaging spectrometer data. *Remote Sens Environ* 1995;54:127–40.
- [45] Dozier J. Spectral signature of alpine snow cover from the Landsat Thematic Mapper. *Remote Sens Environ* 1989;28:9–22.
- [46] Liston GE, Elder K. A distributed snow-evolution modeling system (SnowModel). *J Hydrometeorol* 2006;7:1259–76.
- [47] Groot Zwaaftink CD, Löwe H, Mott R, Bavay M, Lehning M. Drifting snow sublimation: a high-resolution 3-D model with temperature and moisture feedbacks. *J Geophys Res* 2011;116:D16107.
- [48] Fang X, Pomeroy JW. Modelling blowing snow redistribution to prairie wetlands. *Hydrol Process* 2009;23:2557–69.
- [49] Hiemstra CA, Liston GE, Reiners WA. Observing, modelling, and validating snow redistribution by wind in a Wyoming upper treeline landscape. *Ecolog Model* 2006;197:35–51.
- [50] Link T, Marks D. Distributed simulation of snow cover mass- and energy-balance in the boreal forest. *Hydrol Process* 1999;13:2439–52.
- [51] Garen DC, Marks D. Spatially distributed energy balance snowmelt modelling in a mountainous river basin: estimation of meteorological inputs and verification of model results. *J Hydrol* 2005;315:126–53.
- [52] Marks D, Winstral A. Comparison of snow deposition, the snow cover energy balance, and snowmelt at two sites in a semiarid mountain basin. *J Hydrometeorol* 2001;2:213–27.
- [53] Marks D, Link T, Winstral A, Garen D. Simulating snowmelt processes during rain-on-snow over a semi-arid mountain basin. *Ann Glaciol* 2001;32:195–202.
- [54] Goodison BE, Louie PYT, Yang D. WMO solid precipitation measurement intercomparison, Final Report. World Meteorological Organization, Geneva, Switzerland, 1998. pp. 318.
- [55] Winstral A. Spatial scaling of snow processes: modelling implications [PhD. thesis]. Reading, UK: University of Reading; 2011.
- [56] Schmidt RA. Properties of blowing snow. *Rev Geophys Space Phys* 1982;20:39–44.
- [57] Li L, Pomeroy JW. Estimates of threshold wind speeds for snow transport using meteorological data. *J Appl Meteorol* 1997;36:205–13.
- [58] Doorschot J, Lehning M, Vrouwe A. Field measurements of snow drift threshold and mass fluxes, and related model simulations. *Boundary-Layer Meteorol* 2004;113:347–68.
- [59] Pomeroy JW, Toth B, Granger RJ, Hedstrom NR, Essery RL. Variation in surface energetics during snowmelt in a subarctic mountain catchment. *J Hydrometeorol* 2003;4:702–19.
- [60] Erxleben J, Elder K, Davis R. Comparison of spatial interpolation methods for estimating snow distribution in the Colorado Rocky Mountains. *Hydrol Process* 2001;16:3627–49.
- [61] Elder K, Michaelsen J, Dozier J. Small basin modeling of snow water equivalence using binary regression tree methods, In: K.A. Tonnissen, M.W. Williams, M. Tranter (Eds.), *Biogeochemistry of seasonally snow-covered catchments IAHS-AIHS and IUGG XX general assembly*, Boulder, Colorado, July 1995, IAHS Publication No 228/1995 129–139.
- [62] Balk B, Elder K. Combining binary decision tree and geostatistical methods to estimate snow distribution in a mountain watershed. *Water Resour Res* 2000;36:13–26.
- [63] Mason SJ. *Seasonal and Longer-Range Forecasts*. John Wiley & Sons Ltd: Forecast Verification; 2011. pp. 203–220.
- [64] Flerchinger GN, Cooley KR, Ralston DR. Groundwater response to snowmelt in a mountainous watershed. *J Hydrol* 1992;133:293–311.
- [65] Nash JE, Sutcliffe JV. River flow forecasting through conceptual models Part I – A discussion of principles. *J Hydrol* 1970;10:282–90.
- [66] Liston GE, Elder K. A meteorological distribution system for high-resolution terrestrial modeling. *J Hydrometeorol* 2006;7:217–34.
- [67] MacDonald RJ, Byrne JM, Kienzle SW. A physically based daily hydrometeorological model for complex mountain terrain. *J Hydrometeorol* 2009;10:1430–46.
- [68] Running SW, Nemani RR, Hungerford RD. Extrapolation of synoptic meteorological data in mountainous terrain and its use for simulating forest evapotranspiration and photosynthesis. *Canadian J Forest Resour* 1987;17:472–83.
- [69] Daly C, Halbleib M, Smith JL, Gibson WP, Doggett MK, Taylor GH, et al. Physiographically sensitive mapping of climatological temperature and precipitation across the conterminous United States. *Int J Climatol* 2008;28:2031–64.
- [70] Marshall HP, Koh G. FMCW radars for snow research. *Cold Regions Sci Technol* 2008;52:118–31.
- [71] Heilig A, Eisen O, Schneebeli M. Temporal observations of a seasonal snowpack using upward-looking GPR. *Hydrol Process* 2010;24:3133–45.